ACS OMEGA

http://pubs.acs.org/journal/acsodf

Article

Synthesis of Zinc Oxide Eudragit FS30D Nanohybrids: Structure, Characterization, and Their Application as an Intestinal Drug Delivery System

Fan Luo, Mingjie Wang, Liting Huang, Ziqian Wu, Wenxiong Wang, Ayesha Zafar, Yunbo Tian, Murtaza Hasan,* and Xugang Shu*

Cite This: *ACS Omega* 2020, 5, 11799−11808

Read Online

ACCESS | Metrics & More | Article Recommendations

ABSTRACT: The present study was designed to develop multifunctional zinc oxide-encapsulated Eudragit FS30D (ZnO/EFS) nanohybrid structures as a biodegradable drug delivery system and as a promising successful carrier for targeting sites. The solvent evaporation method was used to fabricate the ZnO/EFS nanohybrids and the size, shape, stability, and antioxidant activity were characterized using transmission electron microscopy (TEM), scanning electron microscopy (SEM), X-ray diffraction (XRD), Fourier transform infrared (FTIR) spectroscopy, dynamic light scattering (DLS), thermogravimetric analysis (TGA), and an antioxidant (1,1-diphenyl-2-picrylhydrazyl (DPPH)). Zinc oxide-encapsulated Eudragit FS30D (ZnO/EFS) nanohybrid structures consisted of irregularly shaped, 297.65 nm-sized ZnO/EFS microcapsule, enduring thermal stability from 251.17 to 385.67 °C. Nano-ZnO was encapsulated in EFS through the formation of hydrogen bonds, and the average encapsulation efficiency for nano-ZnO was determined to be 96.12%. In vitro intestinal-targeted drug release assay provided 91.86% with free nano-ZnO, only 9.5% in acidified ZnO/EFS nanohybrid structure but the rate ZnO/EFS nanohybrids reached 93.11% in succus entericus resultantly modified nano-ZnO was proven proficient intestinal-specific delivery system. The stability of the ZnO/EFS nanohybrid structures was confirmed using ζ-potential and antioxidant activity analysis. Hence, the EFS nanoencapsulation strategy of ZnO provided a stable, nontoxic, and pharmacokinetically active intestine-specific system that can become the best choice for an effective oral feed additive in future.

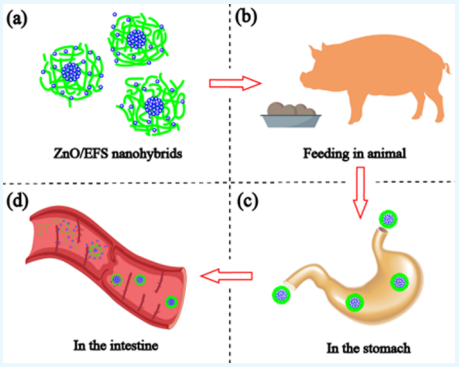

INTRODUCTION

With an increase in global population, and an associated increase in per capita meat consumption, the higher pasture intensities have become an inevitable choice for us, with the avoidance of further deforestation and grassland conversion.[1] Pasture intensification reduced the area needed for livestock and poultry, but improving the physical fitness of animals became a key technical requirement.[2] Indeed, there is considerable evidence that animal health is related to feed conversion efficiency.[3] Animals require essential dietary intake regularly as the trace micronutrients do not sustain for a longer period of time for the vital functions of the body such as metabolism, growth, and reproduction.[4−6] To date, the most crucial task for specialized ranchers has been formulating an effective method for improving the animal quality via enhancing the feed efficiency.[7,8] Therefore, the importance of improving the efficiency and pharmacokinetics of the additives used in animal feeds has become more evident.

Nano-ZnO, being the new feed Zn supplement source, has the potential to enhance the growth performance and immune status in animals, due to its small size and versatile surface chemistry.[9−11] It has been reported that dietary zinc oxide nanoparticles at a level of 30 mg/kg could improve the immune and antioxidant status of *Oreochromis niloticus*.[12] Also, previous reports demonstrated that nano-ZnO supplementation could modulate protein abundances in blood plasma and the intestine of common carp (*Cyprinus carpio*).[13,14] However, the bioavailability of nano-Zn is still unsatisfactory. The uncoated nano-Zn does not fulfill the bioavailability criteria as it gets easily degraded and then excreted by any change in the physiological condition such as the acidic pH, high ionic strength, etc.[15] Studies have also shown the poor resistivity of the nano-ZnO within the gastric fluid and the short residence time in the intestine that makes it incompetent to get absorbed into the body.[16] Moreover, the complexes of nano-ZnO remain undigested and unprocessed due to the presence of

Received: March 18, 2020
Accepted: May 4, 2020
Published: May 13, 2020

https://dx.doi.org/10.1021/acsomega.0c01216
ACS Omega 2020, 5, 11799−11808

endogenous inhibitors in feed diets (tricalcium phosphate, phytic acid, and fiber).[17] If the nano-ZnO was completely dissolved during the acid dissolution process, then no significant difference should be seen between the nano-ZnO and inorganic forms ($ZnCl_2$).[18] Further, the ZnO chelation with amino acids improves its bioavailability that can help to increase the functionality. Besides, this organic zinc in animal diets is limited due to its insignificance.[19,20] Correspondingly, excess Zn leads to pollution of urban runoff and aquatic systems, which have an adverse effect on sustainable land management and future biodiversity conservation.[21,22] Therefore, there is an urgent need for finding new ways that could enhance the oral bioavailability of nano-ZnO.

Over the past decades, biodegradable polymeric materials have made the most outstanding contribution to human autoimmunity and tumor therapy as ideal drug delivery systems.[23,24] Biodegradable polymeric materials exhibited good stability, tolerability, and longer circulation in previous biological trials.[25−27] It has been shown that a biodegradable polymeric system can cross the biological barriers (e.g., the gastrointestinal tract and blood vessels) and control drug release to targeted cancer sites via some modification of its components.[28,29] Further optimization for the targeted drug delivery in previous studies had been achieved by changing the pH, time, or pressure.[30] As in many cases, the release of drugs from a drug delivery system can be controlled on an ideal time scale and at a specific site, to allow more accurate and complete absorption of drugs into the body.[27,31] For drugs that are directly released at the target tissue, dosing frequency and drug side effects are reduced.[32] An example is the site-specific drug delivery as in intestine cancer that is considered effective and more applicable.[33] Therefore, a feasible nanotechnological method that would contribute to promoting the bioavailability of nano-ZnO was provided in this work. Therefore, a contrasting combination of such biodegradable polymers and nanovectors needs to be united to form a single platform that could increase the biocompatibility and thus increase the bioavailability in a specific drug delivery system.

Eudragit FS30D (EFS) is a terpolymer that was composed of methacrylic acid, methyl acrylate, and methyl methacrylate. Due to the presence of methacrylic groups, the solubility of EFS in aqueous solution is pH-dependent.[34] The combination of these repeating units within this polymer formed the basic skeleton of the protective shell of the drug under harsh physiological conditions (stomach environment).[35] Once the EFS coating−drug system moves into the gastrointestinal tract, the drug will optimally be absorbed depending on the properties of the encapsulating shell and better bioavailability.[36] As a pH- and time-sensitive polymer, EFS has been widely used in the medical and food industries. It has been reported that drugs that can be delivered via using EFS include proteins, flavonoids, and small-molecule particles.[23] Moreover, since EFS is an approved pharmaceutical excipient, the nano-ZnO delivery system can be tailored by EFS.[37]

In the present study, a biodegradable polymeric material Eudragit FS30D (EFS) was used as the drug delivery vehicle to synthesize ZnO/EFS nanohybrids. The encapsulated ZnO/EFS provides a different surface chemistry that stabilizes and increases the bioavailability of the ZnO. This strategy provides an excellent source of a nanoencapsulated thermally stable additive that provides boosted drug storage and delivery capacity.

RESULTS AND DISCUSSION

Encapsulation Efficiency (EE) of Nanoparticles. In some sense, an orthogonal experiment has considerable potential to scan all of the parameters systematically in an efficient way with a minimum computational load.[38] It has several advantages such as uniformly distributed points for data collection, minimization of experiments for comprehensive analysis, and convenient range and variance analysis.[39] In this experiment, the influential factors of the fabrication conditions mainly include the weight of EFS (A), the rotational speed (B), the amount of Span 80 (C), and the dose of magnesium stearate (D). Each factor had three levels indexed from 1 to 3, which denoted the chosen values of the operation parameters. According to the orthogonal experiment theory, the range method was used to analyze the significance level of the factors. K_{Jm} represents the sum of the EE of the m level of column J factors, where the J value represents the experimental factors and the m value represents the experimental levels. Besides, k_{Jm} stands for the average of the K_{Jm} ($k_{Jm} = K_{Jm}/3$). According to the k_{Jm}, the R value was calculated by $R_J = k_{J,\max} - k_{J,\min}$. R_J was the range of column J factors, which responded to the fluctuation of each level. The greater the R values, the greater is the encapsulation efficiency.[40]

The EE (%) of the four factors of nano-ZnO is shown in Table 1. Obviously, the preparation of ZnO/EFS nanohybrids show a good EE for nano-ZnO, where the EE is generally above 90%. In the experiment, four factors were arranged as A > D > B > C according to the R values. The result of the orthogonal experiment showed that the dosage of EFS plays an important role in the preparation of ZnO/EFS nanohybrids. Since EFS is the basic skeleton of the nanoparticle coating, it would decrease the surface Gibbs free (δG) energy and reduce the surface tension, thereby increasing the overall mechanical strength and protecting the drugs in the capsule core.[41]

Table 1. Orthogonal Experiment Design and Nano-ZnO Entrapment Efficiency EE (%)

	experimental factors				
entry	A	B	C	D	EE (%)
1	1	1	1	1	93.43
2	1	2	2	2	96.24
3	1	3	3	3	98.96
4	2	1	2	3	95.22
5	2	2	3	2	93.71
6	2	3	1	1	99.50
7	3	1	3	2	91.88
8	3	2	1	3	91.11
9	3	3	2	1	90.21
K_1	288.63	280.53	284.04	283.14	
K_2	288.43	281.06	281.67	281.83	
K_3	273.2	288.67	284.55	285.29	
k_1	96.21	93.51	94.68	94.38	
k_2	96.14	93.68	93.89	93.94	
k_3	91.06	96.22	94.85	95.09	
R	5.14	2.72	0.96	3.42	

An insufficient or excessive dosage of EFS affected the physicochemical properties (e.g., polarity and surface tension) of the solution during preparation, which affected the EE of ZnO/EFS nanohybrids.[42] In addition, it has been observed that an overdosage of EFS can also reduce the EE of ZnO/EFS

https://dx.doi.org/10.1021/acsomega.0c01216
ACS Omega 2020, 5, 11799−11808

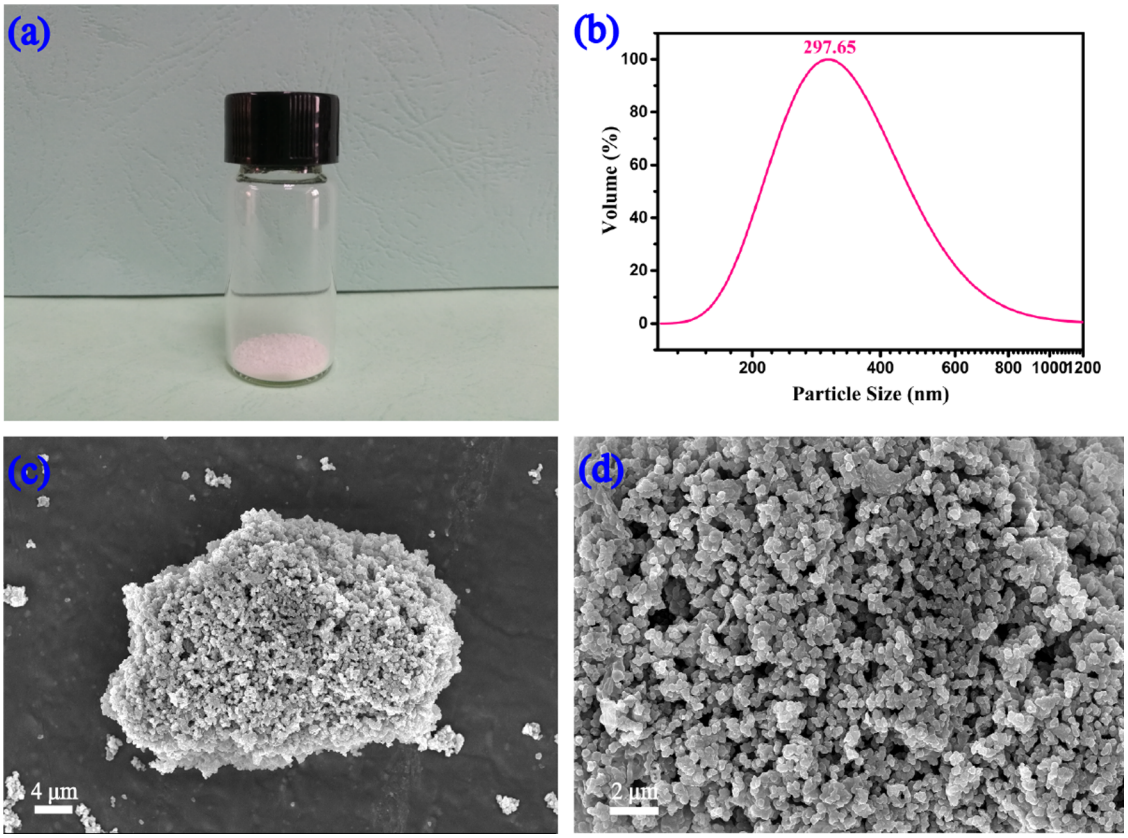

Figure 1. Morphology and microstructure of ZnO/EFS nanohybrids: (a) photographic image, (b) particle size, and (c, d) SEM image.

nanohybrids. The main reason is that EFS is an anionic copolymer.[34] Thus, an excessive amount of EFS would increase the electrostatic repulsion between EFS and nano-ZnO, which would have a negative effect on the encapsulation processes. Simultaneously, EFS gets clustered and does not encapsulate nano-ZnO due to its strong self-polymerization.[43]

According to the analytical results of the orthogonal experiment, the optimized formulation, $A_1B_3C_3D_3$, was 0.20 g of EFS, the centrifugation during emulsification was conducted at 700 rpm, the amount of Span 80 was 0.45 g, and the dose of magnesium stearate was 0.035 g. Under these conditions, the average encapsulation efficiency of the obtained nanoparticles from the five experimental groups was 96.12% (SD = 0.676).

Morphological Observation. As shown in Figure 1a, the ZnO/EFS nanohybrids were white powder with a uniform color. However, the texture of ZnO/EFS nanohybrids was not as fine as nano-ZnO, which was mainly due to the difference in their microstructure and material composition. To further analyze the microstructure, ZnO/EFS nanohybrids were investigated by dynamic light scattering (DLS), as shown in Figure 2b. It is interesting to note that the monodispersed nanoparticles were obtained in this experiment with a relatively unified size distribution. The average particle size of ZnO/EFS nanohybrids was measured to be 297.65 nm, as shown in Figure 1b. The scanning electron microscopy (SEM) image showed the uniform size of ZnO/EFS nanohybrids, which is depicted in Figure 1c.

This expected observation was mainly contributed by the Span 80, which reduced the dielectric constant and led to the removal of the hydration of EFS, which ultimately reduced the surface tension force of EFS.[44,45] It is noteworthy that a

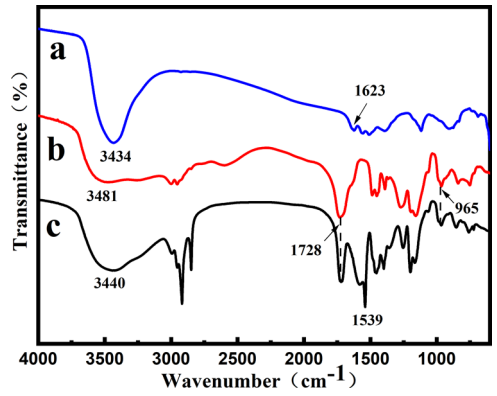

Figure 2. Fourier transform infrared (FTIR) characterization: (a) nano-ZnO, (b) EFS, and (c) ZnO/EFS nanohybrids.

suitable proportion of raw material and the correct method are also crucial for the size of nanoparticles.[46] Moreover, some large particles were observed, which formed multiple nanoparticles based on the electrostatic interaction.[47,48] As shown in Figure 1d, the irregular shape of ZnO/EFS nanohybrids was also investigated by a scanning electron microscope. This phenomenon can be related to the undirected bridging and by the distortions of the polymer chains of EFS.[49]

FTIR Analysis. To reveal the encapsulation mechanism of the carriers, nano-ZnO, EFS, and ZnO/EFS nanohybrids were subjected to FTIR spectroscopy, as shown in Figure 2. From spectra a in Figure 2, we noticed that crystalline water is present in nano-ZnO molecules from the O−H peak at 3434 and 1623 cm^{-1}.[50] This means that nano-ZnO has a tendency to form hydrogen bonds with EFS. In Figure 2b, an absorption

https://dx.doi.org/10.1021/acsomega.0c01216
ACS Omega 2020, 5, 11799−11808

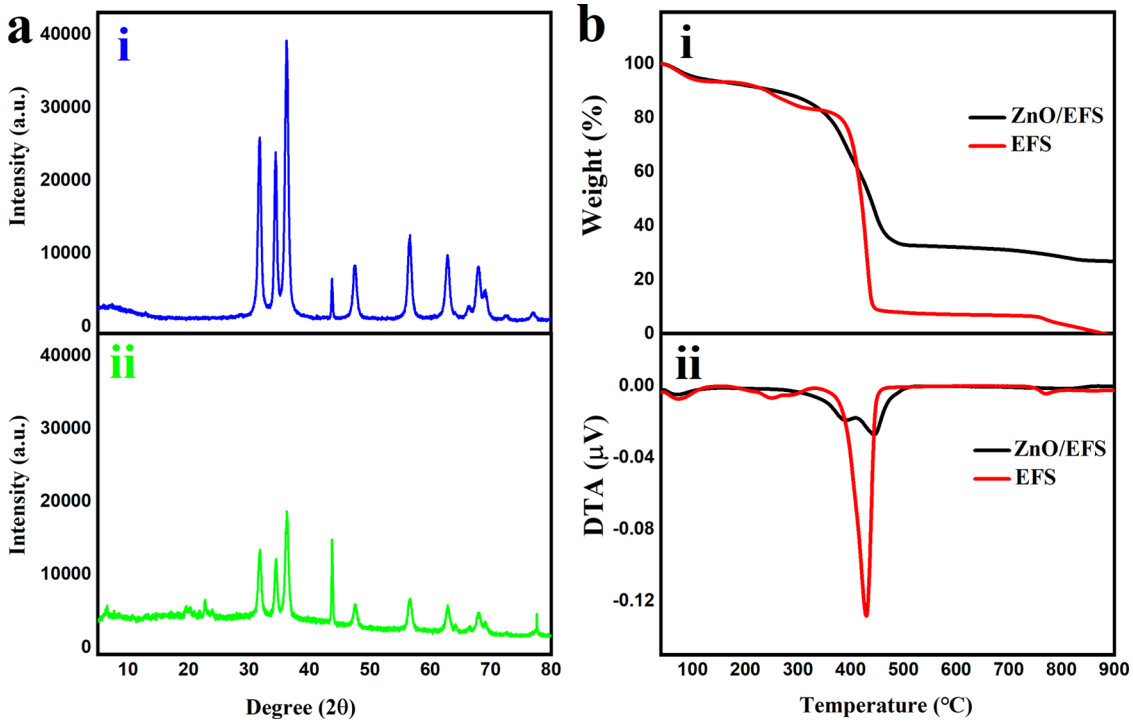

Figure 3. Physicochemical characterization: (a) XRD patterns: (i) nano-ZnO and (ii) ZnO/EFS nanohybrids; and (b) thermograms: (i) thermogravimetry (TG) curves and (ii) derivative thermogravimetry (DTA) curves.

peak is observed at 3481 cm^{-1}, which is attributed to the stretching vibration absorption peak of the −OH group of the surface of EFS.[51]

In addition, the peak at 1728 cm^{-1} could be ascribed to the stretching vibrations of C═O.[35] Furthermore, the quaternary ammonium groups of EFS gave rise to the characteristic peak at 965 cm^{-1}.[52] For the last c spectra shown in Figure 2, a significant change was observed in the characteristic peak, which indicated that the EFS was involved in the intermolecular interaction. A new absorption peak appeared at 1539 cm^{-1} due to EFS attachment of additional carbonyl groups of EFS to nano-ZnO through hydrogen bonds.[37] This indicated that nano-ZnO could be successfully encapsulated into the nanoparticles due to the functionally active groups held on the surface and the protruding groups that provide stable interaction and binding sites.

X-ray Diffraction (XRD) and Thermogravimetric Analysis (TGA). To further evaluate the ZnO/EFS nanohybrid interactions, ZnO/EFS nanohybrids and nano-ZnO were investigated by XRD, as shown in Figure 4a. For nano-ZnO (Figure 3ai), a series of intense and sharp Bragg peaks appeared at 2θ values of 31.77, 34.42, 36.25, 47.54, 56.60, 62.86, 67.96, 69.10, 72.56, and 76.95°, which corresponds to those in the report of Hu.[53] Simultaneously, it is interesting to note that the Bragg peaks of nano-ZnO are also found in the XRD spectra of the ZnO/EFS nanohybrids at the same diffraction angles, as shown in Figure 3aii. This indicates that the entire encapsulating process did not destroy the structure and crystal phase of the nano-ZnO. Moreover, the diffraction peak intensity of the ZnO/EFS nanohybrids appears to be reduced compared to that of the nano-ZnO, and some additional low-intensity and unrecognizable amorphous-phase peaks are even found. This could be an indication of amorphization due to EFS being an amorphous material.[49] Besides, this phenomenon points out the possibility that the nano-ZnO release is principally controlled by ZnO/EFS nanohybrids.

Figure 3bi shows the TG analysis results for EFS and ZnO/EFS nanohybrids. Like EFS, the first decomposition event of ZnO/EFS nanohybrids from 40 to 150 °C was caused by free water and crystal water evaporation. However, compared with EFS, which showed a weight loss of 5.59 wt %, the ZnO/EFS nanohybrids had almost no loss of weight from 250 to 320 °C. Simultaneously, the thermal stability of ZnO/EFS nanohybrids improved from 251.17 to 385.67 °C, as shown in DTA curves (Figure 3bii). This phenomenon could be ascribed to the formation of hydrogen bonds within ZnO/EFS nanohybrids such that the energy was increased to remove the dimethylamino group and to form the six-membered cyclic anhydride.[54,55] Besides, EFS and ZnO/EFS nanohybrids had a large weight loss at 320−500 °C due to the complete decomposition of the next terpolymer.[52] Correspondingly, the highest decomposition temperatures of EFS and ZnO/EFS nanohybrids were observed at 429.83 and 444.67 °C from DTA curves, respectively. Moreover, it was worth noting that the mass loss of EFS reached 100% at 900 °C and the weight reduction of ZnO/EFS nanohybrids was only 74%. Due to the excellent thermal stability of nano-ZnO, this observation further proved that the nano-ZnO could be successfully loaded into the nanoparticles.

In Vitro Release Study. To evaluate the ability of products to control the release of nano-ZnO, the in vitro release experiments of free nano-ZnO and ZnO/EFS nanohybrids under gastrointestinal tract mimicking conditions (pH = 1.0/6.8) were conducted. As shown in Figure 4, it was clear that ZnO/EFS nanohybrids can effectively protect nano-ZnO from separating out in the simulation of gastric fluid. Simultaneously, the drug system of ZnO/EFS nanohybrids guarantees the sustained release of nano-ZnO in the simulation of a succus entericus environment.

https://dx.doi.org/10.1021/acsomega.0c01216
ACS Omega 2020, 5, 11799−11808

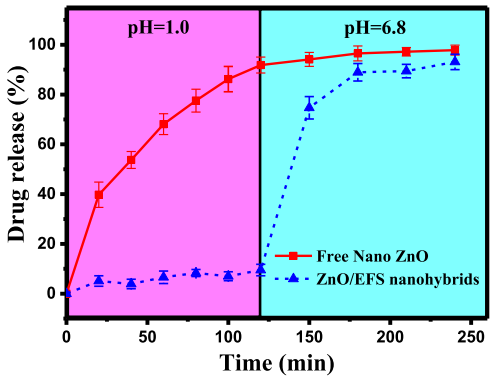

Figure 4. Drug release of free nano-ZnO and ZnO/EFS nanohybrids.

At pH = 1.0, the drug release of free nano-ZnO was found to be higher at first, and the cumulative release rate even increased rapidly to 91.86% after 120 min. In contrast, the cumulative release rate of ZnO/EFS nanohybrids was only 9.5%. With the pH changed to 6.8, interesting results were observed with the drug release for ZnO/EFS systems. The cumulative release rate of ZnO/EFS nanohybrids was found to rapidly increase to 74.7% after 150 min. And the total release rate of ZnO/EFS nanohybrids was 93.11% after the end of the experiment, which was close to that of the free nano-ZnO (97.85%).

In the entire in vitro release test, these expected results could be ascribed to the special structure of EFS. Theoretically speaking, the nanoparticle coating was not destroyed in the acidic medium due to the EFS acidity coefficient of 7.5.[37] Thus, it could be observed that only a small amount of nano-ZnO was released from the ZnO/EFS system in the simulation of gastric fluid. However, the carboxylic acid groups of EFS get ionized with the increase in the surrounding pH.[56] When the electrostatic repulsion generated based on the deprotonated carboxylic acid groups is stronger than the drug−polymer interaction, ZnO/EFS systems collapse and thus promote the continuous release of nano-ZnO in the simulation of the succus entericus environment.[57] Figure 5 shows a similar mechanism of ZnO/EFS nanohybrids in animals.

Like humans, the gastric fluid and the succus entericus of most mammals were proved to be at pH 1.0 and 6.8, respectively.[58] Therefore, the in vitro drug release study reveals that the ZnO/EFS nanohybrids are confirmed to be an intestine-targeted drug system. The intestine-specific delivery of nano-ZnO would allow it to be more accurately and completely absorbed via the intestinal tissues, thereby greatly improving the bioavailability of nano-ZnO. Simultaneously, the existence of ZnO/EFS nanohybrids will effectively avoid unwanted systemic absorption and side effects (e.g., inflammation and oxidative stress) caused by a burst drug release.[59,60] Overall, the ability of good gastroresistance and intestinal targeting makes ZnO/EFS nanohybrids an ideal drug delivery system.

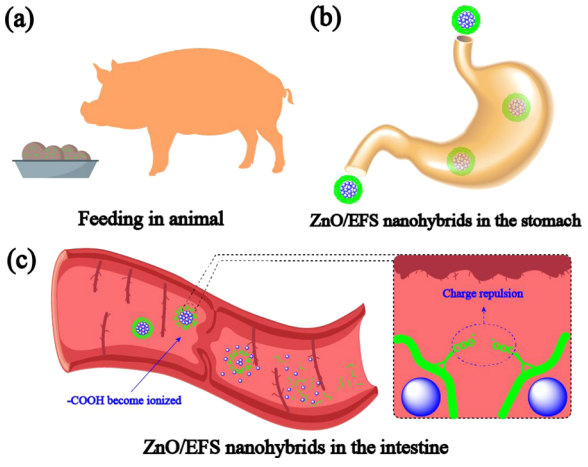

Figure 5. Possible schematic diagram of the mechanism of ZnO/EFS nanohybrids in animals (a−c) PC: Fan Luo.

Antioxidant Activity Study. 1,1-Diphenyl-2-picrylhydrazyl (DPPH) was widely used to evaluate the antioxidation activity of materials due to its stability and sensitivity. The more the DPPH radical is cleared, the stronger is the antioxidant.[61] When the DPPH solution is mixed with a substance that can provide electrons or hydrogen atoms, the electrons on the oxygen atoms of the DPPH radical will be transferred to the odd electrons of the nitrogen atom, thereby losing the original violet color and reducing its own absorbance.[9] Therefore, the antioxidant activity of ZnO/EFS nanohybrids (or nano-ZnO) was tested by DPPH in a further set of experiments. On treatment, the drug delivery system did not alter the antioxidant properties of the nano-ZnO, as shown in Figure 6.

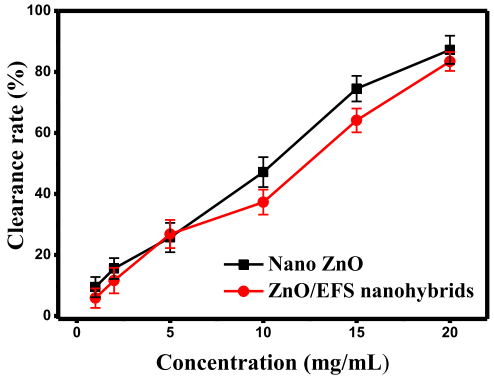

Figure 6. DPPH radical-scavenging capacity of nano-ZnO and ZnO/EFS nanohybrids.

It was observed that the antioxidation activity with different concentrations between ZnO/EFS nanohybrids and nano-ZnO was quite similar. The maximum DPPH clearance of the ZnO/EFS microcapsule was 83.43%, which was close to that of the free nano-ZnO (87.24%). On the other hand, compared to nano-ZnO, a slight reduction in the antioxidant activity of ZnO/EFS nanohybrids may occur due to the loss of antioxidants with poor stability, which has also been observed in previous reports.[15,62]

Storage Stability Study. In the packaging and storage of feed, the external environment, including the temperature and humidity, can influence the stability and physiological efficacy of nano-ZnO.[63] Thus, it is important to evaluate the storage stability of ZnO/EFS nanohybrids prepared in this work. As shown in Figure 7a,b, it is clear that the particle size and ζ-potential of ZnO/EFS nanohybrids do not change significantly under normal storage conditions (25 °C/60% relative humidity (RH)) for 1 month.

https://dx.doi.org/10.1021/acsomega.0c01216
ACS Omega 2020, 5, 11799−11808

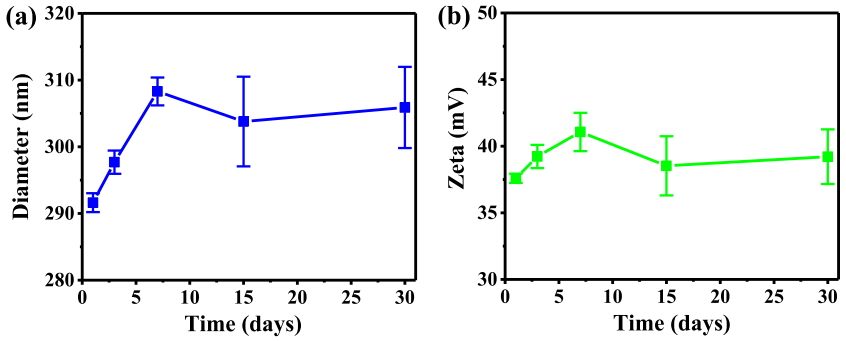

Figure 7. Storage stability of ZnO/EFS nanohybrids: (a) DLS size changes and (b) ζ-potential changes.

The average particle size of ZnO/EFS nanohybrids increased from 291.63 to 305.89 nm, and its ζ-potential increased from 37.59 to 39.21 mV. This expected result could be caused by the encapsulation process that could reduce the surface energy and charge density of nano-ZnO, preventing nanoparticles from clustering with each other.[49] Therefore, this implies that ZnO/EFS nanohybrids could stabilize and extend the shelf life of nano-ZnO.

CONCLUSIONS

EFS-nanoencapsulated ZnO showed a tectonic melioration in the bioavailability and pharmacokinetics of less operable nano-ZnO. According to the structural characterization such as FTIR, XRD, and TG, nano-ZnO was confirmed to be successfully encapsulated in EFS through the construction of hydrogen bonds. Moreover, the irregular shape of ZnO/EFS nanohybrids was observed by using SEM. The average particle size of ZnO/EFS nanohybrids was 297.65 nm, measured via DLS. The cumulative release rate of ZnO/EFS nanohybrids was found to be only 9.5% in the gastric fluid. In contrast, the cumulative release rate of ZnO/EFS nanohybrids was found to be rapidly increased to 93.11% in the succus entericus by the in vitro release test. Hence, gastroresistance and intestine-targeted ZnO/EFS nanohybrids allowed nano-ZnO to get absorbed completely. It was also concluded that ZnO/EFS nanohybrids inherited the original antioxidant activity of nano-ZnO, which ensured the normal biochemical function of nano-ZnO in animals. A storage stability study was conducted to monitor the stability and the shelf life of nano-ZnO. Conclusively, the nontoxic and stable ZnO/EFS nanohybrids, as a drug delivery unit, have great potential for improving the bioavailability and retaining the biochemical function of nano-ZnO in animal nutrition and may serve as an effective alternative for animal feed in future.

MATERIALS AND METHODS

Nano-ZnO (GR, size: 30 ± 10 nm) was kindly donated by Shanghai Maikun Chemical Ltd. EFS (Evonik Industries AG, Germany) was purchased from Sandoz Ltd. Span 80 was prepared by Shanghai Jingchun Biochemical Technology Ltd. Magnesium stearate was supplied by Tianjin Fucheng Chemical Reagent Factory. All other chemicals in this experiment were of analytical grade and used as received.

Preparation of Nano-ZnO-Encapsulated Eudragit FS30D (ZnO/EFS) Nanohybrids. In this work, the ZnO/EFS nanohybrids were synthesized by the solvent evaporation (single emulsion) method, as described previously.[64] Briefly, 0.2 g of EFS was weighed and dissolved in 12 mL of ethyl alcohol to obtain an aqueous phase. Span 80 (450 mg), magnesium stearate (35 mg), and nano-ZnO (0.3 g) were solubilized in 15 mL of paraffin, and the oil phase was obtained in a water bath at room temperature. Then, the aqueous phase was added dropwise into the oil phase under magnetic stirring. After 60 min, the mixture solution was stirred gently for 30 min at 80 °C to remove the residual ethanol. Finally, the solid product was washed with *n*-hexane at least three times to remove the superfluous paraffin. Eventually, the nanoparticles were obtained by vacuum-drying at 50 °C for 1 day. The fabrication process of ZnO/EFS nanohybrids is outlined in Figure 8.

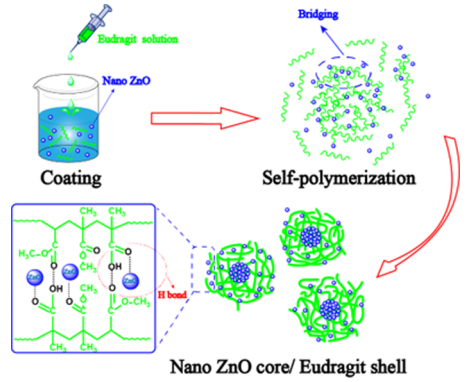

Figure 8. Schematic representation for the synthesis of ZnO/EFS nanohybrids.

Design of Orthogonal Experiment. An orthogonal test is a useful and effective measurement for assaying the comprehensive effect of a large number of environmental factors on the encapsulation efficiency (EE). To investigate the effect of fabrication conditions on nanoparticles and to obtain the best product, four factors in three levels were studied based on the EE as the evaluation index.[39] An L9 (3^4) orthogonal experiment on the weight of EFS named A, the rotational speed named B, the amount of Span 80 named C, and the dose of magnesium stearate named D was designed and is shown in Table 2.

Encapsulation Efficiency Performance Test. Ten milligrams of ZnO/EFS nanohybrids was weighed and charged into a 20 mL beaker to be mixed with 10 mL of 0.1 mol/L HCl for 10 min under magnetic stirring. Then, the solution was transferred to a volume flask after filtration and diluted to 100 mL with deionized water. Free zinc content was measured and calculated by using an inductively coupled plasma spectrom-

https://dx.doi.org/10.1021/acsomega.0c01216
ACS Omega 2020, 5, 11799−11808

Table 2. Factors and Levels of the Orthogonal Experiment

	factors			
levels	EFS (g) (A)	rotational speed (rpm) (B)	Span 80 (g) (C)	magnesium stearate (g) (D)
1	0.2	500	0.35	0.025
2	0.3	600	0.40	0.030
3	0.4	700	0.45	0.035

eter (ICP 2100, PerkinElmer). At the same time, the encapsulation efficiency of nano-ZnO was calculated as follows

$$\mathrm{EE}\ (\%) = \frac{W_{\mathrm{total}} - W_{\mathrm{free}}}{W_{\mathrm{total}}} \quad (1)$$

where W_{total} represents the weight of zinc in nano-ZnO initially added to the formulation, and W_{free} is the weight of zinc in unentrapped nano-ZnO.

Physicochemical Structural and Morphological Analyses. Nano-ZnO, EFS, and ZnO/EFS nanohybrids were analyzed in the range of 600−4000 cm^{-1} via a Fourier transform infrared (FTIR) spectrometer (Spectrum 100, PerkinElmer Inc.). XRD analysis of nano-ZnO and ZnO/EFS nanohybrids at 5−80° was performed using an X-ray powder diffractometer (X'Pert PRO MPD, Panalytica, Holland). Under the protection of nitrogen, the thermal stability of EFS and ZnO/EFS nanohybrids at 40−900 °C was investigated by a thermogravimetric analyzer (TGA2, Mettler Toledo, Switzerland). Five milligrams of ZnO/EFS nanohybrids was scattered in deionized water, and then the sample solution was dripped and dried on the silicon wafer stage. After the surface of the samples was sprayed with gold particles, a scanning electron microscope (EVO18, Mettler) was used to observe the morphology and particle size of the sample. After the ZnO/EFS nanohybrids were scattered in deionized water, dynamic light scattering (90 Plus PALS, Brookhaven) was used to measure the particle size and ζ-potential of the sample.

In Vitro Drug Release Study. This work is mainly based on the in vitro drug release research method reported by a previous study, and the specific operation is as follows.[49] Seven hundred and fifty milligrams of the acidic medium simulating the gastric fluid (0.1 M HCl, pH 1.0) was prepared and transferred to the dissolution vessel. According to the operational requirements of the dissolution tester (RC12AD, TDTF, China), the mechanical paddle was adjusted to the most suitable rotational speed and height. Then, 1 g of ZnO/EFS nanohybrids (or nano-ZnO) was placed in a dissolution vessel and kept in an incubator beaker throughout this work (37 °C). After the start of the experiment, 5 mL of sample solution was collected in the glass tube every 20 min, and the lost solution was supplied automatically by the machine. After 2 h, 250 mL of 0.2 mol/L of phosphate buffer was added to the dissolution vessel to change the pH of the solution to 6.8 (succus entericus). At the specified time (30 min) intervals, 5 mL of samples was collected, and the missing phosphate buffer was supplied automatically by the machine. The experiment was terminated after 2 h. All of this work was carried out in triplicate.

One milliliter of sample solutions was accurately placed from the glass tube to a volume flask and diluted to 100 mL with deionized water. Free zinc content was measured and calculated by using the ICP (ICP 2100, PerkinElmer). Meanwhile, the release rate of zinc in nano-ZnO was calculated as follows

$$Q_n\ (\%) = \frac{V_s \sum_{k=1}^{n-1} c_k + V_r c_n}{W} \quad (2)$$

where V_s is the measured volume of the sample, V_r represents the volume of the medium, c represents the zinc content measured by ICP, n is the number of samples, and W is the drug loading of 1 g of ZnO/EFS nanohybrids.

Antioxidation Capacity Assay. To test the antioxidant activity of products, nano-ZnO and ZnO/EFS nanohybrids were investigated via 1,1-diphenyl-2-picrylhydrazyl (DPPH) free radical-scavenging activity assay.[63] Briefly, 25 μL of different concentrations of ZnO/EFS nanohybrids (or nano-ZnO) was added to 2 mL of the DPPH ethanol solution (50 μg/mL). Then, the mixed solutions were stored at room temperature in the dark. After 60 min, the mixed solution was measured by an ultraviolet spectrophotometer (UV-2550, Shimadzu, Japan) at λ = 524 nm. All of this work was carried out in triplicate. Besides, the clearance rate (C) of DPPH was calculated as follows

$$C\ (\%) = \left(1 - \frac{A - A_1}{A_0}\right) \times 100 \quad (3)$$

where A is the measured absorbance of the reaction mixture of samples with the DPPH solution, A_1 represents the absorbance of the solutions of samples without DPPH, and A_0 is the initial absorbance of DPPH without the samples.

Storage Stability Analysis. According to the International Conference on Harmonization (ICH) guideline, the stability of ZnO/EFS nanohybrids under storage conditions of 25 °C and 60% relative humidity (RH) was investigated for 1 month.[64] Dynamic light scattering was used to measure the particle size and ζ-potential of the sample for a period of 1, 3, 7, 15, and 30 days. All of this work was carried out in triplicate.

AUTHOR INFORMATION

Corresponding Authors

Murtaza Hasan − *School of Chemistry and Chemical Engineering, Zhongkai University of Agriculture and Engineering, Guangzhou 510225, China; Department of Biochemistry & Biotechnology (Baghdad-ul-Jadeed Campus), The Islamia University of Bahawalpur, Bahawalpur 63100, Pakistan;* orcid.org/0000-0001-7715-9173; Phone: 86-020-8900-3114; Email: murtaza@iub.edu.pk

Xugang Shu − *School of Chemistry and Chemical Engineering, Zhongkai University of Agriculture and Engineering, Guangzhou 510225, China; Guangdong Province Key Laboratory of Waterfowl Healthy Breeding, Guangzhou 510225, China;* Email: xgshu@21cn.com

Authors

Fan Luo − *School of Chemistry and Chemical Engineering, Zhongkai University of Agriculture and Engineering, Guangzhou 510225, China*

Mingjie Wang − *School of Chemistry and Chemical Engineering, Zhongkai University of Agriculture and Engineering, Guangzhou 510225, China*

Liting Huang − *School of Chemistry and Chemical Engineering, Zhongkai University of Agriculture and Engineering, Guangzhou 510225, China*

Ziqian Wu − *School of Chemistry and Chemical Engineering, Zhongkai University of Agriculture and Engineering, Guangzhou 510225, China*

https://dx.doi.org/10.1021/acsomega.0c01216
ACS Omega 2020, 5, 11799−11808

Wenxiong Wang − *School of Energy and Environment and State Key Laboratory of Marine Pollution, City University of Hong Kong, Kowloon 999077, Hong Kong, China*
Ayesha Zafar − *Department of Biochemistry & Biotechnology (Baghdad-ul-Jadeed Campus), The Islamia University of Bahawalpur, Bahawalpur 63100, Pakistan*
Yunbo Tian − *School of Chemistry and Chemical Engineering, Zhongkai University of Agriculture and Engineering, Guangzhou 510225, China; Guangdong Province Key Laboratory of Waterfowl Healthy Breeding, Guangzhou 510225, China*

Complete contact information is available at:
https://pubs.acs.org/10.1021/acsomega.0c01216

Notes

The authors declare no competing financial interest.

■ ACKNOWLEDGMENTS

The authors express their gratitude for the financial support from the Guangdong−Hong Kong Cooperation Project (2017A050506055), the Guangdong Provincial Education Department Project (Natural Science, 2017KZDXM045), the Agriculture and Rural Department Project of Guangdong Province, the Guangzhou Foreign Cooperation Project (201907010033), the Graduate Technology Innovation Fund (KJCX2019004), and the Undergraduate Innovation and Entrepreneurship Training Program (S201911347028).

■ REFERENCES

(1) Alexandratos, N.; Bruinsma, J. In *World Agriculture towards 2030/2050: The 2012 Revision*, ESA Working Paper 12-03, 2012; pp 1−146.
(2) Erb, K.-H.; Lauk, C.; Kastner, T.; Mayer, A.; Theurl, M. C.; Haberl, H. Exploring the biophysical option space for feeding the world without deforestation. *Nat. Commun.* **2016**, *7*, No. 11382.
(3) Styles, D.; Gonzalez Mejia, A.; Moorby, J.; Foskolos, A.; Gibbons, J. Climate mitigation by dairy intensification depends on intensive use of spared grassland. *Global Change Biol.* **2018**, *24*, 681−693.
(4) Chen, K.; Jiang, W.; Wu, P.; Liu, Y.; Kuang, S.; Tang, L.; Tang, W.; Zhang, Y.; Zhou, X.; Feng, L. Effect of dietary phosphorus deficiency on the growth, immune function and structural integrity of head kidney, spleen and skin in young grass carp (*Ctenopharyngodon idella*). *Fish Shellfish Immunol.* **2017**, *63*, 103−126.
(5) Gao, X.; Tang, B.; Liang, H.; Yi, L.; Wei, Z. Selenium deficiency induced an inflammatory response by the HSP60 - TLR2-MAPKs signalling pathway in the liver of carp. *Fish Shellfish Immunol.* **2019**, *87*, 688−694.
(6) Zheng, J.; Luo, Z.; Hu, W.; Liu, C.; Chen, Q. Differential effects of dietary Zn deficiency and excess on carnitine status, kinetics and expression of CPT I in yellow catfish *Pelteobagrus fulvidraco*. *Aquaculture* **2014**, *420*−*421*, 10−17.
(7) Kreidenweis, U.; Humpenöder, F.; Kehoe, L.; Kuemmerle, T.; Bodirsky, B. L.; Lotze-Campen, H.; Popp, A. Pasture intensification is insufficient to relieve pressure on conservation priority areas in open agricultural markets. *Global Change Biol.* **2018**, *24*, 3199−3213.
(8) Williams, D. R.; Alvarado, F.; Green, R. E.; Manica, A.; Phalan, B.; Balmford, A. Land-use strategies to balance livestock production, biodiversity conservation and carbon storage in Yucatán, Mexico. *Global Change Biol.* **2017**, *23*, 5260−5272.
(9) Mishra, P. K.; Mishra, H.; Ekielski, A.; Talegaonkar, S.; Vaidya, B. Zinc oxide nanoparticles: a promising nanomaterial for biomedical applications. *Drug Discovery Today* **2017**, *22*, 1825−1834.
(10) Akbar, S.; Haleem, K. S.; Tauseef, I.; Rehman, W.; Ali, N.; Hasan, M. *Raphanus sativus* mediated synthesis, Characterization and Biological Evaluation Zinc Oxide Nanoparticles. *Nanosci. Nanotechnol. Lett.* **2017**, *9*, 2005−2012.
(11) Hasan, M.; Ullah, I.; Zulfiqar, H.; Naeem, K.; Iqbal, A.; Gul, H.; Ashfaq, M.; Mahmood, N. Biological entities as chemical reactors for synthesis of nanomaterials: Progress, challenges and future perspective. *Mater. Today Chem.* **2018**, *8*, 13−28.
(12) Awad, A.; Zaglool, A. W.; Ahmed, S. A. A.; Khalil, S. R. Transcriptomic profile change, immunological response and disease resistance of *Oreochromis niloticus* fed with conventional and Nano-Zinc oxide dietary supplements. *Fish Shellfish Immunol.* **2019**, *93*, 336−343.
(13) Chupani, L.; Zusková, E.; Niksirat, H.; Panáček, A.; Lünsmann, V.; Haange, S.; von Bergen, M.; Jehmlich, N. Effects of chronic dietary exposure of zinc oxide nanoparticles on the serum protein profile of juvenile common carp (*Cyprinus carpio* L.). *Sci. Total Environ.* **2017**, *579*, 1504−1511.
(14) Chupani, L.; Niksirat, H.; Lünsmann, V.; Haange, S.; von Bergen, M.; Jehmlich, N.; Zuskova, E. Insight into the modulation of intestinal proteome of juvenile common carp (*Cyprinus carpio* L.) after dietary exposure to ZnO nanoparticles. *Sci. Total Environ.* **2018**, *613*−*614*, 62−71.
(15) Caddeo, C.; Gabriele, M.; Fernàndez-Busquets, X.; Valenti, D.; Fadda, A. M.; Pucci, L.; Manconi, M. Antioxidant activity of quercetin in Eudragit-coated liposomes for intestinal delivery. *Int. J. Pharm.* **2019**, *565*, 64−69.
(16) Swinkels, J. W.; Kornegay, E. T.; Verstegen, M. W. Biology of zinc and biological value of dietary organic zinc complexes and chelates. *Nutr. Res. Rev.* **1994**, *7*, 129−149.
(17) Wang, H.; Zhu, H.; Wang, X.; Li, E.; Du, Z.; Qin, J.; Chen, L. Comparison of copper bioavailability in copper-methionine, nano-copper oxide and copper sulfate additives in the diet of Russian sturgeon *Acipenser gueldenstaedtii*. *Aquaculture* **2018**, *482*, 146−154.
(18) Wang, J.; Wang, A.; Wang, W. Evaluation of nano-ZnOs as a novel Zn source for marine fish: importance of digestive physiology. *Nanotoxicology* **2017**, *11*, 1026−1039.
(19) Zhao, C.; Tan, S.; Xiao, X.; Qiu, X.; Pan, J.; Tang, Z. Effects of Dietary Zinc Oxide Nanoparticles on Growth Performance and Antioxidative Status in Broilers. *Biol. Trace Elem. Res.* **2014**, *160*, 361−367.
(20) Kazemi, E.; Sourinejad, I.; Ghaedi, A.; Johari, S. A.; Ghasemi, Z. Effect of different dietary zinc sources (mineral, nanoparticulate, and organic) on quantitative and qualitative semen attributes of rainbow trout (*Oncorhynchus mykiss*). *Aquaculture* **2020**, *515*, No. 734529.
(21) Northey, S. A.; Mudd, G. M.; Werner, T. T.; Jowitt, S. M.; Haque, N.; Yellishetty, M.; Weng, Z. The exposure of global base metal resources to water criticality, scarcity and climate change. *Global Environ. Change* **2017**, *44*, 109−124.
(22) Röös, E.; Bajželj, B.; Smith, P.; Patel, M.; Little, D.; Garnett, T. Greedy or needy? Land use and climate impacts of food in 2050 under different livestock futures. *Global Environ. Change* **2017**, *47*, 1−12.
(23) Hasan, M.; Ayesha, Z.; Maryam, Y.; Huma, G.; Kinza, M.; Shahbaz, G. H.; Ayesha, S.; Areeba, Y.; Abeer, M.; Rongji, D.; Nasir, M. Synthesis of Loureirin B-Loaded Nanoliposomes for Pharmacokinetics in Rat Plasma. *ACS Omega* **2019**, *4*, 6914−6922.
(24) Hasan, M.; Iqbal, J.; Awan, U.; Xin, N.; Dang, H.; Waryani, B.; Ullah, K.; Rongji, D.; Deng, Y.; Saeed, Y. LX loaded nanoliposomes synthesis, characterization and cellular uptake studies in H_2O_2 stressed SH-SY5Y cells. *J. Nanosci. Nanotechnol.* **2014**, *14*, 4066−4071.
(25) Dang, H.; Meng, M. H. W.; Zhao, H.; Iqbal, J.; Rongji, D.; Deng, Y.; Lv, F. Luteolin-Loaded Solid lipid nanoparticle synthesis, characterization and improvement of bioavailability, pharmacokinetics invitro and vivo studies. *J. Nanopart. Res.* **2014**, *17*, No. 2347.
(26) Vanderburgh, J.; Hill, J. L.; Gupta, M. K.; Kwakwa, K. A.; Wang, S. K.; Moyer, K.; Bedingfield, S. K.; Merkel, A. R.; d'Arcy, R.; Guelcher, S. A.; et al. Tuning Ligand Density To Optimize Pharmacokinetics of Targeted Nanoparticles for Dual Protection against Tumor-Induced Bone Destruction. *ACS Nano* **2020**, *14*, 311−327.

(27) Ramírez-García, P. D.; Retamal, J. S.; Shenoy, P.; Imlach, W.; Sykes, M.; Truong, N.; Constandil, L.; Pelissier, T.; Nowell, C. J.; Khor, S. Y.; et al. A pH-responsive nanoparticle targets the neurokinin 1 receptor in endosomes to prevent chronic pain. *Nat. Nanotechnol.* **2019**, *14*, 1150−1159.
(28) Song, W.; Anselmo, A. C.; Huang, L. Nanotechnology intervention of the microbiome for cancer therapy. *Nat. Nanotechnol.* **2019**, *14*, 1093−1103.
(29) Blanco, E.; Shen, H.; Ferrari, M. Principles of nanoparticle design for overcoming biological barriers to drug delivery. *Nat. Biotechnol.* **2015**, *33*, 941−951.
(30) Zhang, S.; Langer, R.; Traverso, G. Nanoparticulate drug delivery systems targeting inflammation for treatment of inflammatory bowel disease. *Nano Today* **2017**, *16*, 82−96.
(31) Osterberg, L.; Blaschke, T. Adherence to Medication. *N. Engl. J. Med.* **2005**, *353*, 487−497.
(32) Kamaly, N.; Yameen, B.; Wu, J.; Farokhzad, O. C. Degradable Controlled-Release Polymers and Polymeric Nanoparticles: Mechanisms of Controlling Drug Release. *Chem. Rev.* **2016**, *116*, 2602−2663.
(33) Zhang, S.; Langer, R.; Traverso, G. Nanoparticulate drug delivery systems targeting inflammation for treatment of inflammatory bowel disease. *Nano Today* **2017**, *16*, 82−96.
(34) Zhang, F. Melt-Extruded Eudragit FS-Based Granules for Colonic Drug Delivery. *AAPS PharmSciTech* **2016**, *17*, 56−67.
(35) Moghimipour, E.; Rezaei, M.; Kouchak, M.; Fatahiasl, J.; Angali, K. A.; Ramezani, Z.; Amini, M.; Abedin, F.; Handali, D. S. Effects of coating layer and release medium on release profile from coated capsules with Eudragit FS 30D: an in vitro and in vivo study. *Drug Dev. Ind. Pharm.* **2018**, *44*, 861−867.
(36) Shah, S. U.; Socha, M.; Sejil, C.; Gibaud, S. Spray-dried microparticles of glutathione and S-nitrosoglutathione based on Eudragit FS 30D polymer. *Ann. Pharm. Fr.* **2017**, *75*, 95−104.
(37) Moustafine, R. I.; Bodrov, A. V.; Kemenova, V. A.; Rombaut, P.; Van den Mooter, G. Drug release modification by interpolymer interaction between countercharged types of Eudragit RL 30D and FS 30D in double-layer films. *Int. J. Pharm.* **2012**, *439*, 17−21.
(38) Fang, S.; Gu, W.; Chen, L.; Yu, Z.; Dai, M.; Lin, Y.; Liao, Y.; Ma, X. Ultrasonic pretreatment effects on the co-pyrolysis of municipal solid waste and paper sludge through orthogonal test. *Bioresour. Technol.* **2018**, *258*, 5−11.
(39) Zhang, Z.; Fang, H.; Yan, H.; Jiang, Z.; Zheng, J.; Gan, Z. Influencing factors of GaN growth uniformity through orthogonal test analysis. *Appl. Therm. Eng.* **2015**, *91*, 53−61.
(40) Wei, L.; Huang, X.; Huang, Z.; Zhou, Z. Orthogonal test design for optimization of lipid accumulation and lipid property in Nannochloropsis oculata for biodiesel production. *Bioresour. Technol.* **2013**, *147*, 534−538.
(41) Li, J.; Lee, I. W.; Shin, G. H.; Chen, X.; Park, H. J. Curcumin-Eudragit E PO solid dispersion: a simple and potent method to solve the problems of curcumin. *Eur. J. Pharm. Biopharm.* **2015**, *94*, 322−332.
(42) Pareta, R.; Brindley, A.; Edirisinghe, M. J.; Jayasinghe, S. N.; Luklinska, Z. B. Electrohydrodynamic atomization of protein (bovine serum albumin). *J. Mater. Sci.: Mater. Med.* **2005**, *16*, 919−925.
(43) Chantasart, D.; Tocanitchart, P.; Wongrakpanich, A.; Teeranachaideekul, V.; Junyaprasert, V. B. Fabrication and evaluation of Eudragit polymeric films for transdermal delivery of piroxicam. *Pharm. Dev. Technol.* **2018**, *23*, 771−779.
(44) Liang, J.; Qian, Y.; Yuan, X.; Leng, L.; Zeng, G.; Jiang, L.; Shao, J.; Luo, Y.; Ding, X.; Yang, Z.; et al. Span80/Tween80 stabilized bio-oil-in-diesel microemulsion: Formation and combustion. *Renewable Energy* **2018**, *126*, 774−782.
(45) Koneva, A. S.; Safonova, E. A.; Kondrakhina, P. S.; Vovk, M. A.; Lezov, A. A.; Chernyshev, Y. S.; Smirnova, N. A. Effect of Water Content on Structural and Phase Behavior of Water-in-Oil (n-Decane) Microemulsion System Stabilized by Mixed Nonionic Surfactants SPAN80/TWEEN80. *Colloids Surf., A* **2017**, *518*, 273−282.
(46) Pradhan, R.; Kim, S. Y.; Yong, C. S.; Kim, J. O. Preparation and characterization of spray-dried valsartan-loaded Eudragit E PO solid dispersion microparticles. *Asian J. Pharm. Sci.* **2016**, *11*, 744−750.
(47) Mohanta, S.; Singh, S. K.; Kumar, B.; Gulati, M.; Kumar, R.; Yadav, A. K.; Wadhwa, S.; Jyoti, J.; Som, S.; Dua, K.; et al. Efficacy of co-administration of modified apple polysaccharide and probiotics in guar gum-Eudragit S100 based mesalamine mini tablets: A novel approach in treating ulcerative colitis. *Int. J. Biol. Macromol.* **2019**, *126*, 427−435.
(48) Xu, B.; Zhang, W.; Chen, Y.; Xu, Y.; Wang, B.; Zong, L. Eudragit L100-coated mannosylated chitosan nanoparticles for oral protein vaccine delivery. *Int. J. Biol. Macromol.* **2018**, *113*, 534−543.
(49) Moustafine, R. I.; Sitenkov, A. Y.; Bukhovets, A. V.; Nasibullin, S. F.; Appeltans, B.; Kabanova, T. V.; Khutoryanskiy, V. V.; Van den Mooter, G. Indomethacin-containing interpolyelectrolyte complexes based on Eudragit E PO/S 100 copolymers as a novel drug delivery system. *Int. J. Pharm.* **2017**, *524*, 121−133.
(50) Zabihi, E.; Babaei, A.; Shahrampour, D.; ArabBafrani, Z.; Mirshahidi, K. S.; Majidi, H. J. Facile and rapid in-situ synthesis of chitosan-ZnO nano-hybrids applicable in medical purposes; a novel combination of biomineralization, ultrasound, and bio-safe morphologyconducting agent. *Int. J. Biol. Macromol.* **2019**, *131*, 107−116.
(51) Jia, D.; Gao, Y.; Williams, G. R. Core/shell Eudragit/poly (ethylene oxide) fibers for site-specific release. *Int. J. Pharm.* **2017**, *523*, 376−385.
(52) Porfiryeva, N. N.; Nasibullin, S. F.; Abdullina, S. G.; Tukhbatullina, I. K.; Moustafine, R. I.; Khutoryanskiy, V. V. Acrylated Eudragit E PO as a novel polymeric excipient with enhanced mucoadhesive properties for application in nasal drug delivery. *Int. J. Pharm.* **2019**, *562*, 241−248.
(53) Hu, C.; Lu, L.; Zhu, Y.; Li, R.; Xing, Y. Morphological controlled preparation and photocatalytic activity of zinc oxide. *Mater. Chem. Phys.* **2018**, *217*, 182−191.
(54) Lin, G.; Zhou, H.; Lian, J.; Chen, H.; Xu, H.; Zhou, X. Preparation of pH-responsive avermectin/feather keratin-hyaluronic acid with anti-UV and sustained-release properties. *Colloids Surf., B* **2019**, *175*, 291−299.
(55) Manimohan, M.; Pugalmani, S.; Sithique, M. A. Biologically active novelN,N,O donortridentate water soluble hydrazide based O-carboxymethyl chitosan Schiff base Cu (II) metal complexes: Synthesis and characterisation. *Int. J. Biol. Macromol.* **2019**, *136*, 738−754.
(56) Dalmoro, A.; Sitenkov, A. Y.; Lamberti, G.; Barba, A. A.; Moustafine, R. I. Ultrasonic atomization and polyelectrolyte complexation to produce gastroresistant shell-core microparticles. *J. Appl. Polym. Sci.* **2016**, *133*, No. 42976.
(57) Dalmoro, A.; Sitenkov, A. Y.; Cascone, S.; Lamberti, G.; Barba, A. A.; Moustafine, R. I. Hydrophilic drug encapsulation in shell-core microcarriers by two stage polyelectrolyte complexation method. *Int. J. Pharm.* **2017**, *518*, 50−58.
(58) Bergeron, N.; Guay, F. Impact of zinc and arginine on antioxidant status of weanling piglets raised under commercial conditions. *Anim. Nutr.* **2019**, *5*, 227−233.
(59) Naeem, M.; Bae, J.; A. Oshi, M.; Kim, M.; Moon, H. R.; Lee, B. L.; Im, E.; Jung, Y.; Yoo, J. colon-targeted delivery of cyclosporine a using dual-functional eudragit Fs30D/Plga nanoparticles ameliorates murine experimentalbcolitis. *Int. J. Nanomed.* **2018**, *13*, 1225−1240.
(60) Marreiro, D.; Cruz, K.; Morais, J.; Beserra, J.; Severo, J.; de Oliveira, A. Zinc and Oxidative Stress: Current Mechanisms. *Antioxidants* **2017**, *6*, No. 24.
(61) Pápay, Z. E.; Kállai-Szabó, N.; Ludányi, K.; Klebovich, I.; Antal, I. Development of oral site-specific pellets containing flavonoid extract with antioxidant activity. *Eur. J. Pharm. Sci.* **2016**, *95*, 161−169.
(62) Mahdavi, S. A.; Jafari, S. M.; Assadpour, E.; Ghorbani, M. Storage stability of encapsulated barberry's anthocyanin and its application in jelly formulation. *J. Food Eng.* **2016**, *181*, 59−66.
(63) Tang, S.; Li, R.; Tan, J.; Wang, Y.; Jiang, Z. One pot synthesis of water-soluble quercetin derived multifunctional nanoparticles with

https://dx.doi.org/10.1021/acsomega.0c01216
ACS Omega 2020, 5, 11799−11808

photothermal and antioxidation capabilities. *Colloids Surf., B* **2019**, *183*, No. 110429.
(64) Jana, U.; Mohanty, A. K.; Manna, P. K.; Mohanta, G. P. Preparation and characterization of nebivolol nanoparticles using Eudragit RS100. *Colloids Surf., B* **2014**, *113*, 269−275.

https://dx.doi.org/10.1021/acsomega.0c01216
ACS Omega 2020, 5, 11799−11808